Photoproduction of jets and the virtual structure of the photon

D.de Florian [1]

Theoretical Physics Division, CERN, CH 1211 Geneva 23, Switzerland
e-mail: deflo@na47sun05.cern.ch

C.García Canal

Laboratorio de Física Teórica, Universidad Nacional de La Plata,
C.C. 67 - 1900 La Plata - Argentina

R.Sassot

Departamento de Física, Universidad de Buenos Aires
Ciudad Universitaria, Pab.1 (1428) Bs.As. - Argentina

Abstract

We compute the ratio between the direct and the resolved photon components of single jet and dijet production in *ep* collisions for the kinematical range covered by the most recent ZEUS data. We analyse the phenomenological consequences of different models for the structure of virtual photons in these observables and compare them with the available data. We also comment on the correlation between the so called x_γ^{obs} and the 'true' x_γ, that can be inferred from the data.

---

[1]On leave of absence from Departamento de Física, Universidad de Buenos Aires, Ciudad universitaria Pab.1 (1428) Bs.As., Argentina

Introduction:

In recent years, different inclusive photon-photon experiments have contributed to unveil the parton content of photons in a program similar to that pursued for the proton. Several sets of parton distribution functions for the photon have been proposed and are periodically refined attaining increasing levels of precision. For a comprehensive review see references [1, 2].

The photoproduction of jets with large transverse energy at HERA [3], has opened the possibility of testing the gluon content of photons and the accuracy of these experiments allows also a clear discrimination between events generated by quasi-real and virtual photons [4]. These improvements make possible the testing of different hypothesis about the photon structure and its dependence on the virtuality scale, such as how the hadronic component of the photon is supressed at high virtuality, as it is usually expected. The details of this dependence were originally thought to be obtainable by means of a purely perturbative approach [5, 6], at least for a restricted kinematical regime. More recently it has been analized with non perturbative models for the hadronic structure of the photon at some definite energy scale [7, 8]. The above mentioned models are the subyacent motivation of the most recent parton distribution parametrizations, whose energy scale dependence is then driven by the inhomogeneus Altarelli-Parisi evolution equations [5].

Both the perturbative and nonperturbative approaches generate photonic parton distributions which differ not only in the dependence on the virtuality scale but also in its quark and gluonic content. They can be compared and their consequences in different observables analysed.

Recently, the ZEUS collaboration have produced for the first time data on dijet photoproduction in ep collisions for different values of the photon vituality [4]. The preliminary data coming from this measurement allows an interesting test for the current ideas on the virtual photon structure in the range of virtualities spanned between 0.10 and 0.55 GeV^2.

In this paper we compute the ratio between the resolved and the direct photon components of dijet photoproduction in ep collisions, already measured at HERA, using different models for the photon content. In doing so, we take into account the non-trivial kinematical cuts inherent to the experi-

mental data. Particularly, we show how the magnitude and the dependence of this ratio in the photon virtuality is fairly reproduced by model dependent parametrizations for the photon, but not by the perturbative approach, at least at leading order, mainly due to the poor gluon content of this last approximation. We also determine the value of $x_\gamma^{threshold}$, the exact photon energy fraction threshold used to define the ratio, that provides the best agreement between theoretical estimates and experiment. This procedure is necessary due to the fact that the data points are obtained using an experimentally defined threshold fraction, x_γ^{obs}, which is not straightforwardly related to the theoretically defined one. In doing this, we find a rather sensible agreement between the determinations coming from the most realistic parametrizations.

We also compute predictions for the same ratio but for single jet cross sections, as suggested in ref [7], but in an integrated kinematical range, similar to that covered by ZEUS data analyses. For this single jet cross sections, we find a clear increase in the ratio, i.e. in the resolved component, due to low x_γ contributions, which would suggest an increased sensitivity on the gluon component. However, the dependence on the virtuality scale is similar to that of dijet production.

In the following section we define the cross sections to be analysed, specifing the kinematical range over which these are integrated in order to be compared with the experimental data. Then, we make a short summary about the photonic parton distributions to be used and compare their main features. In the third section we show theoretical estimates, compare them with the available data and discuss about the $x_\gamma^{threshold}$ choices that bring the best accord between them. Finally we sumarize our results and present our conclusions.

Jet Cross Sections:

In leading order the differential cross section for two jet production in ep collisions takes a very simple form when written in terms of the fraction of the photon energy intervening in the hard process, x_γ, the fraction of the proton energy carried by the participating parton, x_p, and that of the

2

electron carried by the photon, z [9]

$$\frac{d\sigma}{dx_\gamma \, dx_p \, dz \, dp_T \, dP^2} = \tilde{f}_{\gamma/e}(z, P^2) f^\gamma(x_\gamma, Q^2, P^2) f^p(x_p, Q^2) \frac{d\hat{\sigma}}{dp_T} \qquad (1)$$

Here, p_T is the transverse momentum of the jets, P^2 is the photon virtuality, and Q^2 is the relevant energy scale of the proccess, in this case taken to be equal to p_T^2. $d\hat{\sigma}/dp_T$ represents the hard parton-parton and parton-photon cross sections [10].

The functions $f^\gamma(x_\gamma, Q^2, P^2)$ and $f^p(x_p, Q^2)$ denote the parton distribution functions for the photon and the proton, respectively. The first one reduces to $\delta(1 - x_\gamma)$ -the probability for finding a photon in a photon- for direct contributions, i.e. those in which the photon participates as such in the hard process. $\tilde{f}_{\gamma/e}(z, P^2)$ is the unintegrated Weizsäcker-Williams distribution [11]

$$\tilde{f}_{\gamma/e}(z, P^2) = \frac{\alpha}{2\pi} \frac{1}{P^2} \frac{1 + (1 - z)^2}{z} \qquad (2)$$

which has been shown to be a very good approximation for the distribution of photons in the electron, provided the photon virtuality is much smaller than the relevant energy scale [7].

The differential cross section in eq.(1) can also be written in terms of the (pseudo) rapidities η_1 and η_2, which are constrained by the experimental settings, and the electron and proton energies E_e and E_p [12]. Both pairs of variables are related to the energy fractions by

$$
\begin{aligned}
x_p &= \frac{p_T}{2E_p} \left(e^{\eta_1} + e^{\eta_2}\right) \\
x_\gamma &= \frac{p_T}{2zE_e} \left(e^{-\eta_1} + e^{-\eta_2}\right)
\end{aligned}
\qquad (3)
$$

Kinematical restrictions constrain x_γ to lay in the interval $[p_T^2/x_p z E_e E_p, x_\gamma^{max}]$, x_p in $[p_T^2/z E_e E_p x_\gamma^{max}, 1]$ and z in $[p_T^2/E_e E_p, 1]$. In the ZEUS data there are also additional constraints involved such as those coming from the cuts applied to the rapidities $-1.125 \leq \eta \leq 1.875$, and the ones for the Jacquet-Blondel variable $0.15 \leq y_{JB} \leq 0.75$, which corresponds to $0.20 \leq z \leq 0.80$ [3]. In order to analyse the P^2 dependence of the total cross section, the variables x_γ, x_p, z, and p_T, must be integrated taking into account both sets of constraints.

3

Switching from the (η_1, η_2) plane (figure 1a) to the $(\tilde{x}_p, \tilde{x}_\gamma)$ (figure 1b) where $\tilde{x}_p = x_p 2E_p/p_T$ and $\tilde{x}_\gamma = x_\gamma 2zE_e/p_T$, the triangle ABC is mapped into the area $A'B'C'$ in figure 1b; the triangle ADC is also mapped into the same region, due to the indistinguishability of events related by an exchange of η_1 and η_2. This implies that when integrating over x_p and x_γ, two partonic events must be considered for each point, the two partonic cross sections coming from the exchange of the Mandelstam variables u and t [13],

$$\frac{d\hat{\sigma}}{dp_T} = \frac{d\hat{\sigma}}{dp_T}(s, u, t) + \frac{d\hat{\sigma}}{dp_T}(s, t, u) \tag{4}$$

For dijet process the η cuts applied determine the regions $A'B'C'$ and $A'D'C'$ in the (x_p, x_γ) plane which have to be further constrained with the above mentioned kinematical cuts. For single jets events, due to the η restrictions, only the areas where neither of the jets can be detected are excluded so the x_p, x_γ region is extended with the areas limited by the prolongation of the curves $A'B'$ and $B'C'$

Experimentally, the ratio between the resolved and the direct contributions is defined as the number of events with photon energy fractions x_γ lower than certain threshold value $x_\gamma^{threshold}$ divided by the number of those events with greater energy fractions. Naively, one would expect the direct contribution sharply peaked at $x_\gamma = 1$, i.e. the photon participating with all its energy in the hard process, so the most natural threshold for defining the ratio would be this, however, the detector resolution smears the distribution and also complicates the determination of x_γ, which is then approximated by a measurable fraction x_γ^{obs}, defined in terms of the two highest transverse energy jets. Previous analyses have shown [3] that a threshold of about $x_\gamma^{obs} = 0.75$ provides a good discrimination between direct and resolved events, however it is not possible to determine to which value of the $x_\gamma^{threshold}$ it corresponds [4].

With these elements in mind, one is able to estimate the yield of an experimental determination of the ratio, been the set of photonic parton distributions and the value of $x_\gamma^{threshold}$ the main uncertainties left.

Photonic Parton Distributions:

In recent years, several sets of parton distributions for the real photon have been proposed [1, 2]. The scale dependence of these distributions is driven by the inhomogeneus Altarelli-Parisi evolution equations [5] with input distributions coming from either plausible dynamical assumptions or phenomenological fits to the photon structure function data, as for parton distributions in hadrons. For virtual photons a similar procedure can be followed, provided a dependence on the virtuality scale is somehow implemented. In reference [13], for example, this dependence is introduced, for the quark distributions, by an interpolating factor multiplying the real photon parton distributions

$$r = 1 - \frac{\ln(1 + P^2/P_c^2)}{\ln(1 + Q^2/P_c^2)} \tag{5}$$

where P_c is a typical hadronic scale. For gluons, the factor is chosen to be the square of the former. One can, for example, implement this approach in any of the available real photon parton distributions. Reference [7] proposes a decomposition between a perturbative and a nonperturbative component in the input parton distributions of virtual photons. The former coming from the photon-photon box diagram, whereas the later is related to the parton content of pions. Both contributions are weighted by factors that guarantee a smooth transition to the real photon description. A different decomposition is proposed in reference [8], where the vector meson dominated contribution and the anomalous component are multiplied by certain dipole dampening factors, designed to take into account the P^2 dependence.

Altenatively, virtual photons offer another possibility which consists in obtaining the input parton distributions by a perturbative approach which also takes into account the dependence on the virtuality [6]. The caveat of this approach is that it is only applicable in a restricted kinematical region, ($\Lambda_{QCD}^2 << P^2 << Q^2$), where the photon exhibits hard pointlike behaviour and higher twist corrections can be neglected. In leading order, the resulting parton distributions can then be approximated by

$$q_i^\gamma(x, Q^2, P^2) \simeq \frac{\alpha}{2\pi} 3e_i^2 [x^2 + (1-x)^2] \ln \frac{Q^2}{P^2} \qquad g^\gamma(x, Q^2, P^2) \simeq 0 \tag{6}$$

Next to leading order corrections to these distributions have also been computed finding moderate corrections in the photon structure function but large ones for large values of x [6].

In references [7, 8] it has been noticed that most of the model dependent results for photonic parton distributions are considerably larger than those obtained perturbatively, even in the restricted kinematical region. In order to illustrate this difference, in figure (2a) we show the ratio between the resolved and direct components of dijet photoproduction imposing a threshold value of $x_\gamma = 1.0$ for a fixed value of p_T ($p_T = 4\,GeV$), computed with different parametrizations. The abbreviation 'uem' stands for the perturbative parton distributions of reference [6], 'SaS 1D' and 'SaS 2D' for those of [8], 'GRS' for [7], and 'WHIT#' for those of reference [15] with the implemented P^2 dependence of reference [13]. Clearly, the perturbative distributions yield considerably smaller ratios, the main difference coming from the gluon content, as can be seen in figuere (2b) where the perturbative result is compared with the quark component of the nonperturbative expectation for the ratio.

Experimental Data.

In order to compare theoretical expectations with the available data on dijet photoproduction, it is necesary to find out the x_γ threshold value for the theoretical calculation that corresponds to the x_γ^{obs} of the experiment. At $P^2 = 0.01\,GeV^2$ one would expect photons to behave almost as real photons and the corresponding photonic parton distributions strongly constrained by the real photon data. The model dependence implemented to take into account the virtuality, and the corresponding uncertainty, is then minimised so one can try to find the value of $x_\gamma^{threshold}$ that provides the best accord between the data and the estimates. In figure (3) we show the dijet ratios integrated in p_T and at $P^2 = 0.01\,GeV^2$, as a function of $x_\gamma^{threshold}$ for different sets against the experimental value obtained with $x_\gamma^{obs} = 0.75$ (the thick solid line). The conventions for the other lines are the same as in figures (2a) and (2b). The figure shows that the best value for $x_\gamma^{threshold}$ lays between 0.85 and 0.95. The residual uncertainty in the photonic parton distributions and the experimental errors prevents a more precise determination, however the values coming from most of the distributions are perfectly consistent with the definition of x_γ^{obs}, which implies $0.75 \leq x_\gamma^{threshold} \leq 1.0$. The comparison also rules out some 'extreme' distributions, such as the set WHIT4 [15], which has an enormous gluon component and would require $x_\gamma^{threshold} << 0.75$, or

6

the perturbative set with almost null gluon content ($x_\gamma^{threshold} >> 1$).

In figure (4) we compare the experimental data on dijet with the theoretical expectations coming from different parametrizations as a function of P^2. The lines correspond to the extreme estimates ($x_\gamma^{threshold} = 1.0$ and 0.75, as dashed lines) and to an intermediate value ($x_\gamma^{threshold} = 0.85$, as a solid line). The figures favor distributions with stronger dependence on the virtuality, such as SaS2D and GRS, both of which, incidentally, prefers $x_\gamma^{threshold} \simeq 0.85$. No choice of $x_\gamma^{threshold}$ adjust the estimates coming from other paramentrizations to the data whith similar accuracy. Plausibly, future high statistics data on dijet photoproduction will allow a more stringent discrimination between parton distributions.

In figure (5) we show estimates for single jet ratios. There, the low x_γ contributions coming from the extra integration regions increase the resolved component and thus the value for the ratio. However, the dependence on the virtuality scale and that on the $x_\gamma^{threshold}$, seem to be analogous to those of dijet ratios, implying a similar behaviour of each component inside and outside the restricted A'B'C' region. Apart form this, single jet data would not highlight individual characteristics of the sets, different to those shown by dijet data. However, it can help increasing the statistics of global fits.

7

Conclusions:

We have analysed different estimates for the ratio between direct and resolved contributions for single and dijet photoproduction. We have found a fairly good agreement between the estimates coming from most of the photonic parton distributions available and the data produced by ZEUS, and the impossibility to conciliate these data with the estimates coming from 'extreme' parton distributions, such as those of perturbative origin or with unlikely large gluon content. The P^2-dependent data show greater agreement with estimates coming from parametrizations with stronger P^2 dependence, a large gluon component, and a $x_\gamma^{threshold}$ value of about 0.85, corresponding to $x_\gamma^{obs.} = 0.75$. Single jet ratios show slightly larger resolved components, but a similar P^2 dependence. Future experiments on single jet and dijet photoproduction would be able to further constrain the different proposals for the parton structure in the virtual photon.

Acknowledgements:

8

References

[1] M.Drees, R.Godbole, BU-TH 95/02, hep-ph 9508221, (1995).

[2] T.Sjöstrand, J.K.Storrow, A.Vogt, LU-TP 96-5, hep-ph 9601351, (1996).

[3] M.Derrick et al., Phys.Lett.B322 (1994) 287; B348 (1995) 665;
    T.Ahmed, et al., Nucl.Phys.B445, (1995) 195.

[4] M.L.Utley, GLAS-PPE/95-03, hep-ex 9508016 (1995).

[5] M.Witten, Nucl.Phys.B120, (1977) 189,
    W.A.Bardeen, A.Buras, Phys.Rev.D20, (1976) 166.

[6] T.Uematsu, T.F. Walsh, Phys.Lett. B101, (1981) 263, Nucl.Phys.B199,
    (1982) 93.

[7] M.Gluck, E.Reya, M.Stratmann, DO-TH 96/08 hep-ph 9605297 (1996).

[8] G.Schuler, T.Sjöstrand, CERN-TH/96-04, hep-ph 9601282 (1996).

[9] M.Drees, R.Godbole, Phys.Rev.D39, (1984) 169.

[10] B.L.Combridge et al., Phys.Lett.B70, (1977) 234;
     D.W.Duke, J.Owens, Phys.Rev.D26, (1982) 1600.

[11] S.Frixione, et al., Phys.Lett.B319, (1993) 339.

[12] M.Klasen, G.Kramer, DESY 95-226 (1995).

[13] M.Drees, R.Godbole, Phys.Rev.D50, (1994) 3124.

[14] M.Drees, R.Godbole, Phys.Lett.61, (1988) 683.

[15] K.Hagiwara et al., Phys.Rev.D51, (1995) 3197.

Figure Captions:

Fig.1a Integration regions for the variables η_1 and η_2.

Fig.1b Integration regions for the variables $\tilde{x}_p$ and $\tilde{x}_\gamma$.

Fig.2a The ratio between the resolved and direct components of dijet photo-production ($x_\gamma^{threshold} = 1.0$ and $p_T = 4\,GeV$), computed with different parametrizations.

Fig.2b The same as in Figure (2a) but only for the quark component in the photon.

Fig.3 The dijet ratios integrated in p_T and at $P^2 = 0.01\,GeV^2$ as a function of $x_\gamma^{threshold}$ and for different sets. The experimental value obtained with $x_\gamma^{obs} = 0.75$ is also shown for comparison.

Fig.4 The data on dijet ratios against the theoretical expectations coming from different parametrizations as a function of P^2.

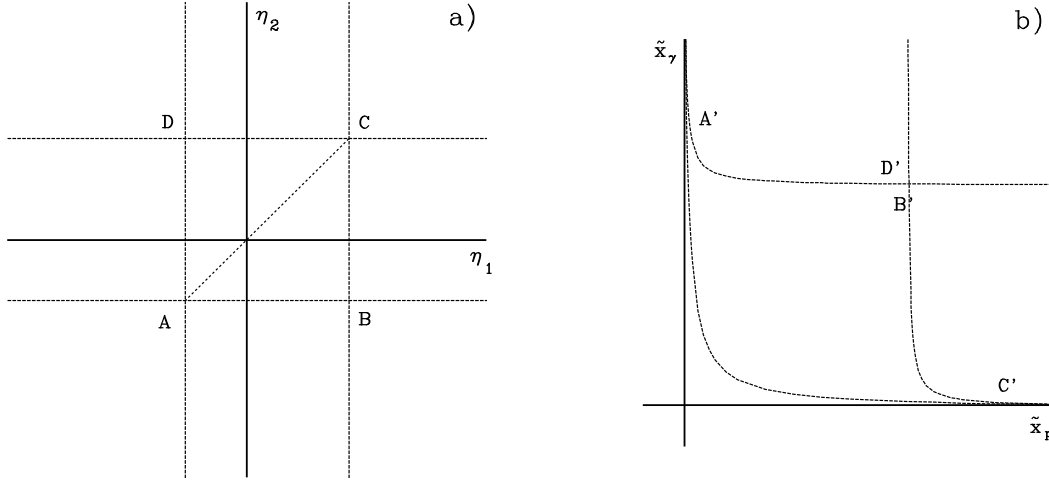**Fig.5** Estimates for single jet ratios as a function of P^2.

10

FIGURE 1

Figure 1: a. Integration regions for the variables η_1 and η_2. b. Integration regions for the variables $\tilde{x}_p$ and $\tilde{x}_\gamma$.
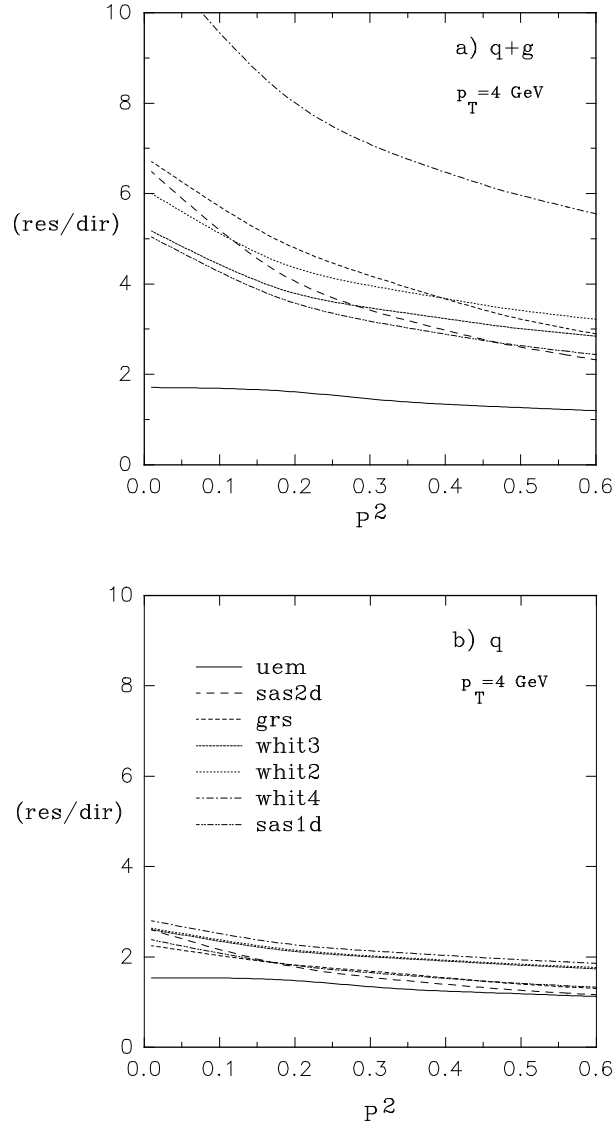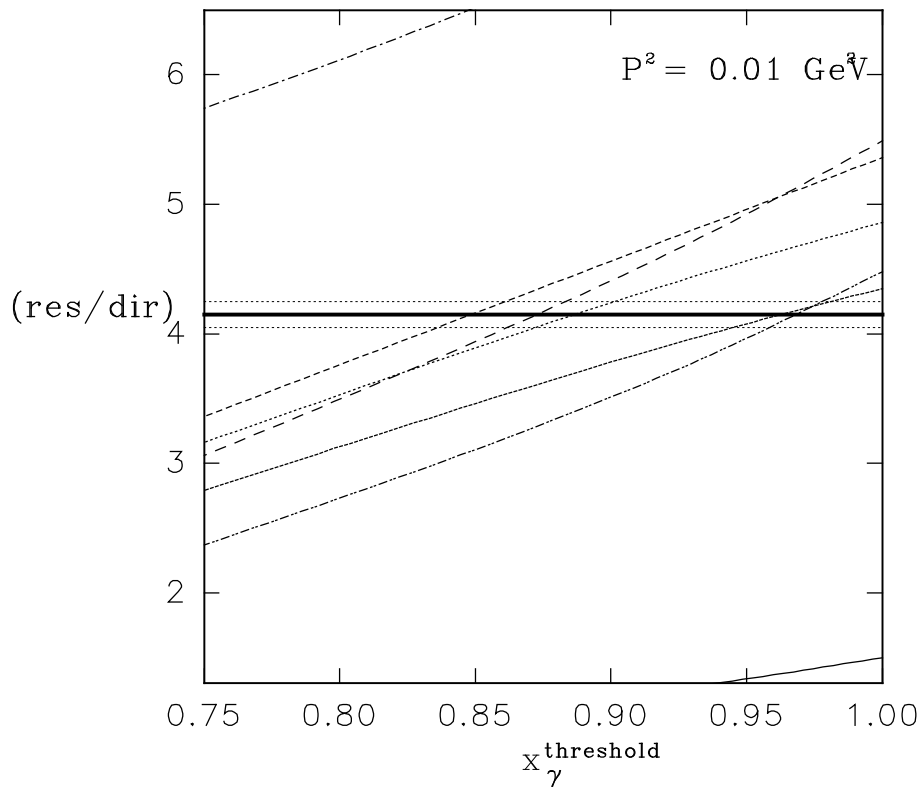
FIGURE 2

Figure 2: a. The ratio between the resolved and direct components of dijet photoproduction $\left(x_\gamma^{threshold} = 1.0 \text{ and } p_T = 4\,GeV\right)$, computed with different parametrizations. b. The same as in Figure (2a) but only for the quark component in the photon.

Figure 3: The dijet ratios integrated in p_T and at $P^2 = 0.01\,GeV^2$ as a function of $x_\gamma^{threshold}$ and for different sets. The experimental value obtained with $x_\gamma^{obs} = 0.75$ is also shown for comparison.
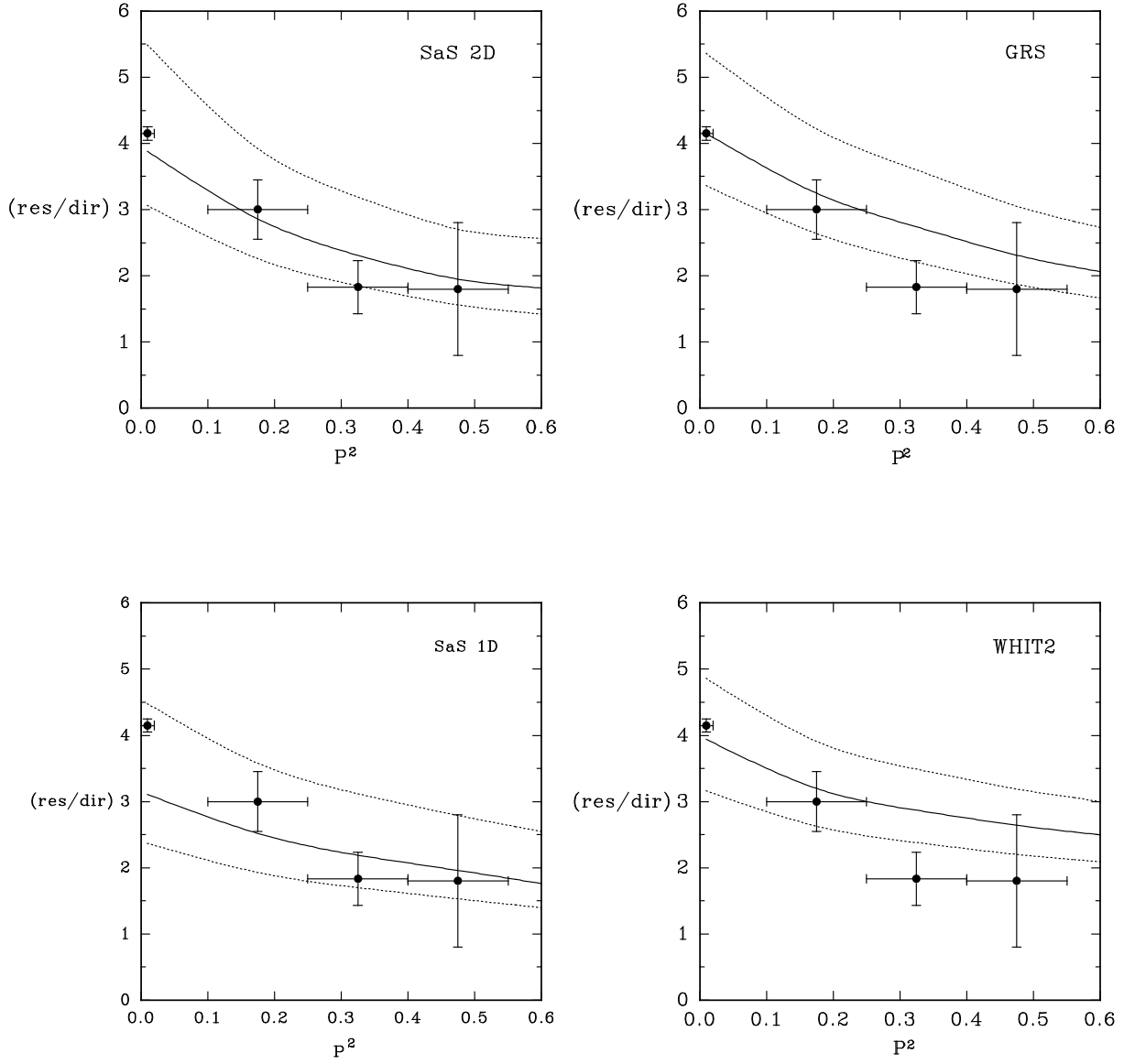
FIGURE 4

Figure 4: The data on dijet ratios against the theoretical expectations coming from different parametrizations as a function of P^2.
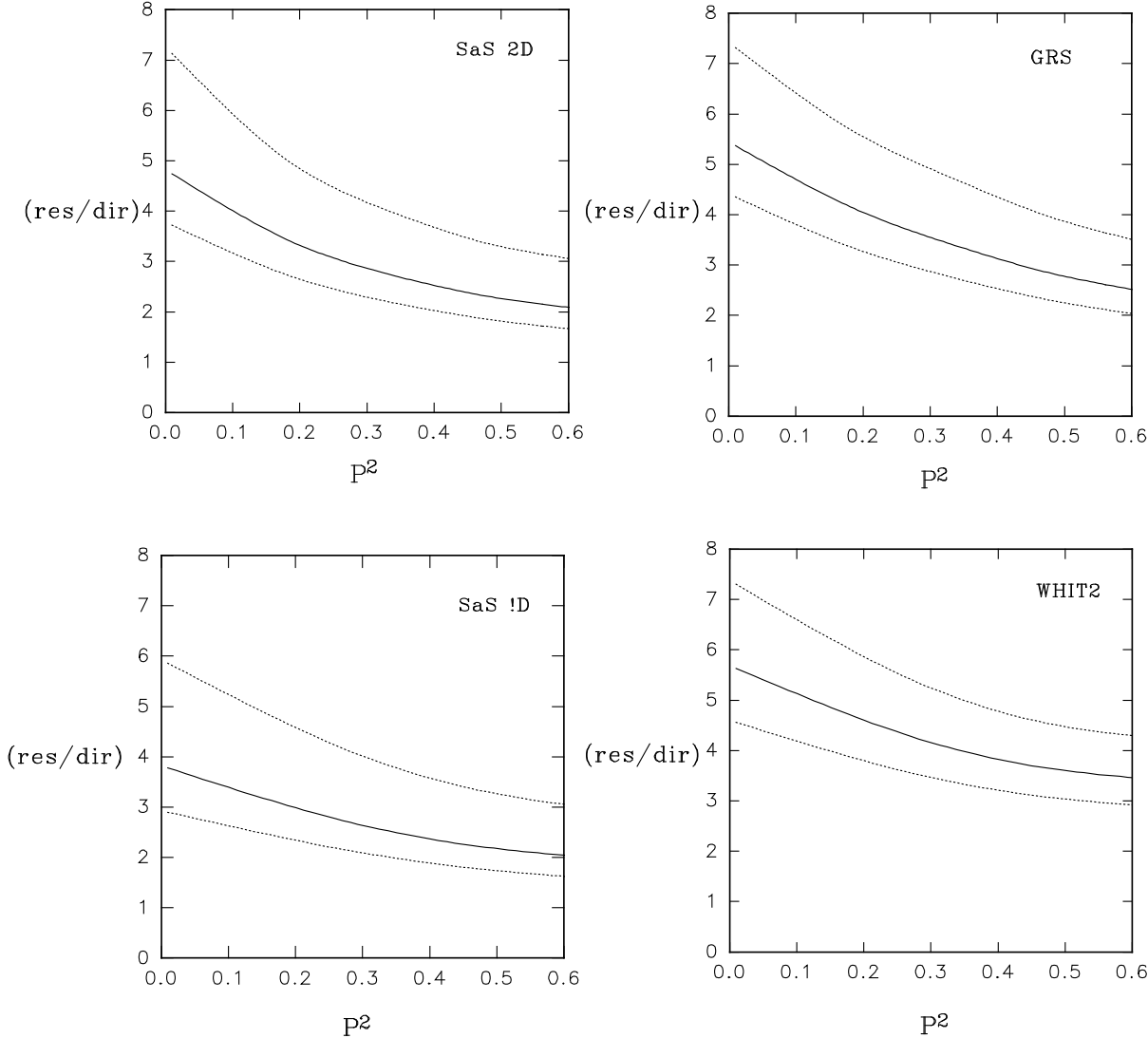
FIGURE 5

Figure 5: Estimates for single jet ratios as a function of P^2.